Fouling-Proof Triple Stream 3D Flow Focusing Based Reactor: Design and Demonstration for Iron Oxide Nanoparticle Co-Precipitation Synthesis

Georgios Gkogkos[a], Maximillian Besenhard[a], Liudmyla Storozhuk[c], Nguyen Thi Kim Thanh[b,c], Asterios Gavriilidis[a]

a. Department of Chemical Engineering, University College London, Torrington Place, London WC1E 7JE, UK
b. Biophysics Group, Department of Physics and Astronomy, University College London, Gower Street, London WC1E 6BT, UK
c. UCL Healthcare Biomagnetic and Nanomaterials Laboratories, University College London, 21 Albemarle Street, London W1S 4BS, UK

Corresponding author: a.gavriilidis@ucl.ac.uk

Abstract

The primary limitation of millifluidic reactors used for (nano)particle synthesis is fouling, which is inherent to small channel devices. This work presents an approach for fouling-free particle production by utilising a novel millifluidic device to achieve a wall-free environment, where the particles are formed. The design was based on CFD simulations and produced a 3-layer co-axial flow in two sequential flow focusing junctions. The device enabled the introduction of a separating stream that prevented premature reaction to avoid fouling at the confluence point. The flow focusing reactor was used for an iron oxide nanoparticle co-precipitation synthesis using tetraethylammonium hydroxide (TEAOH). For this synthesis, it was used to initiate particle formation, and was followed by a millifluidic capillary coil. Fouling resistance at the capillary coil was increased by using excess TEAOH. At elevated temperature (60 ^{o}C) the produced nanoparticles were of superior quality compared to room temperature operation.

Keywords: flow focusing, fouling, nanoparticles, CFD modelling

1. Introduction

Micron and millimetre scale continuous flow devices have emerged as an attractive tool to tame rapid nanoparticle forming processes by offering greatly improved heat and mass transfer rates compared to traditional batch synthesis, resulting in a rapidly achieved highly homogenous reaction environment which is essential for obtaining a high quality product[1–4] . Despite these advantages, the widespread application of small (channel diameters < 1 mm) and compact flow reactors for nanoparticle synthesis is challenged by their inherent difficulty in handling particles. In the confined space of such reactors, solid material accumulation on the walls, known as fouling, can lead to solid depositions comparable in size with the flow channel and thus it may disrupt the flow pattern, reduce residence time and in the worst case, lead to clogging. In nanoparticle forming processes, the most common fouling mechanisms fall into the particulate fouling category as described by Schoenitz et al[5]. Particles formed via crystalisation or precipitation reactions in the proximity of the reactor walls can anchor on the walls where they may act as nucleation points forming larger aggregates that either detach, contaminating the product stream, or grow large enough to clog the channel. Furthermore, free flowing particles may agglomerate into large solid structures, which may deviate from the fluid streamlines, such as in settling at the channel under the effect of gravity or cause clogging via a bridging mechanism[5,6] . Even if the operation of the device is not drastically altered (e.g., in larger millifluidic devices), fouling still might pose a significant problem, affecting the product quality due to secondary nucleation on the channel walls, as has been reported for gold nanoparticle synthesis[7], that affects the chemical species balance or results in material loss.

Many efforts have been made to prevent fouling in small scale flow reactors. Manipulation of hydrodynamics to prevent or reduce particle-wall contact has been demonstrated by using various specially designed reactors. Segmented flow systems[8–10] utilise an immiscible carrier phase which create a thin film between the reactive mixture and the walls, but usually require an additional process step to separate the segmenting fluid from the particle dispersion[11,12]. In single phase systems one way to achieve fouling free nanoparticle synthesis is via free impinging jet reactors[13,14] (IJR) which in addition to offering excellent mixing of reagents, completely remove the need of channels and thus, the possibility of fouling. These characteristics make IJRs an excellent solution for rapid, single stage particle forming processes but restrict their use when multistep processes are considered. Using closed channel reactors for single phase synthesis, can be enabled by manipulating the surface properties of the channels[15,16], but such approaches are typically restricted in simple geometries or involve complicated manufacturing steps, while

their effectiveness may diminish over time. Other strategies focus on controlling the particle-particle and particle-wall interactions from the fluid perspective. Tuning the surface chemistry of the particles by utilizing various ligands enhances colloidal stability of the particles and promotes repulsive particle-particle and particle-wall interactions[17,18] slowing down the onset and growth of fouling. However, these processes typically take place after the initial particle formation and thus cannot prevent fouling during the critical nucleation stage. Repulsive interactions for some particle-wall systems are also expected when operating in basic pH values[5].

Flow focusing devices prevent particle-wall interactions by hydrodynamic confinement of the reactive stream[19–21]. They are of particular interest for nanoparticle synthesis, as their single-phase operation avoids disadvantages of segmented flow, such as the interfacial adsorption of particles[22], does not require phase separation steps, and can be easily integrated into multistep synthetic processes. In addition, by constraining the reaction near the channel centre where the laminar flow velocity profile is nearly flat, the residence time distribution becomes narrower which translates to narrower particle size distributions.[21,23] Typically, flow focusing requires a core stream to be engulfed by a sheath stream, either by using lateral channels as in microfluidic chips[24–26], or with a co-axial capillary configuration[27–29]. Increasing the sheath/core flowrate ratio decreases the width of the core stream, effectively accelerating mixing by diffusion[30]. Although flow focusing reactors have been used to produce a variety of polymeric[25,26,31,32] and inorganic[23, 27,33–36] materials, in most cases they are operated at sub-ml/min flowrates or low particle or reagent concentrations[24,28,29]. In addition, there are reports of fouling at the reactor wall near the confluence point (where the reactants initially meet)[27,37,38] and for two dimensional focusing also at the top and bottom channel walls[25] (both of which have been observed in preliminary experiments, as presented in the SI, section 1). For rapid (nano)particle forming reactions this poses a serious problem, and is only expected to worsen if higher particle concentrations are produced. An interesting (but not widely applied) solution is the introduction of a separating stream between the reactants to prevent premature reaction, as has been demonstrated in a 2D flow focusing microfluidic device[39] and in a multilaminated annular microfluidic device[38].

This work demonstrates a novel triple stream 3D flow focusing millifluidic chip mixer design that introduces a separating stream between the reactants and provides a wall free environment for rapid nanoparticle-producing reactions, effectively eliminating the possibility of fouling. Expanding on existing on-chip flow-focussing devices[25, 32, 36,40,41], this device achieves 3D flow focusing in a single step (junction) and allows the addition of two or more subsequent sheath layers in the same chip, while operating at a wide Reynolds number window with an emphasis on ml/min scale

flowrates, more relevant to high throughput production of materials. The overall device design is based on a simple cross shaped flow focusing chip geometry that is easy to manufacture rapidly and reproducibly with conventional automatable techniques[42] such as computer aided milling, and only requires a two part assembly, overcoming multilayer fabrication challenges often preventing the application of complex on-chip devices. Reproducibility in manufacturing is also an advantage over co-axial capillary devices which produce similar flow patterns, especially when precise sub-mm features are required.

2. Materials and methods

2.1. CFD simulations

Computational fluid dynamic (CFD) simulations assisted the design of a millifluidic mixer geometry that enables complete isolation (in 3D) of the reactive part of the flow (where particles form) from the walls. All finite element method (FEM) simulations were setup using COMSOL Multiphysics 5.4 and solved on a DELL OptiPlex 7060 Windows operated PC with Intel Core i7-8700 CPU and 16 GB of RAM. Multiple simulations were performed, investigating the hydrodynamics of 3D flow focusing for various geometries. Details on the simulations can be found in the SI, section 2.

2.2. Chemicals and materials

The iron precursor solution was prepared by dissolving $FeCl_3 \cdot 6H_2O$ and $FeCl_2 \cdot 4H_2O$ (both from Sigma Aldrich) in deionised (DI) water to a total iron concentration of 0.1 M. The molar ratio was kept at $[Fe^{3+}]/[Fe^{2+}]$ of 2, as it has been shown to produce higher purity magnetite (Fe_3O_4) particles[43,44]. The base solution was prepared by diluting a 20% tetraethylammonium hydroxide (TEAOH) (Sigma Aldrich) solution to a concentration of 0.57 M. HCl stock solution of 1 M (Fisher Scientific) was used for reactor cleaning. A commercial detergent solution (Fairy Ultra 1/20 in DI water) was used to facilitate bubble removal from the device channels in the priming step. Methylene blue (Sigma Aldrich) dissolved in DI water (10 mg/ml) was used for visualisation of the flow pattern in the reactor. 3 mm thickness poly-methyl methacrylate (PMMA) sheets were used for reactor manufacturing as received from DirectPlastics. Araldite Yellow two component epoxy adhesive (Screwfix) was used for sealing the reactor connections.

2.3. Reactor manufacturing

A 3D model of the bottom half of the reactor was designed in Autodesk Inventor 2019 Academic edition. The model was translated in G-code using Inventor's CAM add-on and the pattern was

engraved on two symmetrical PMMA pieces with a Minitek Micromill 3 milling machine. After 1/16" holes were drilled in one of the pieces to accommodate connections to the inlets, the pieces were bonded with a thermally assisted solvent bonding process adapted from[45]. PTFE tubing (*ID* = 1 mm) was connected to the inlet holes via custom made push-fit connections. For the outlet connection, a similar capillary was push-fitted into the outlet port, and a 2-component epoxy adhesive was used to seal the gaps from the square to the cylindrical connection. For the nanoparticle synthesis, the outlet capillary of the triple stream flow focusing chip-mixer was connected to a tightly coiled PTFE capillary (*ID* = 1 mm, length = 15.4 m, volume = 12.1 ml) which provided sufficient residence time for the secondary reaction steps. In the operating regime of interest (Dean number of 3.1-10.6) the coil configuration of the capillary is expected to promote secondary Dean flows that improve the residence time distribution (and thus the homogeneity of the produced particles) by reducing the axial dispersion[46]. Figure S5 in the SI shows the chip device after bonding and the chip-coil assembly used in the high temperature synthesis. More information on manufacturing can be found in the section 3 in the SI.

2.4. Reactor operation

The mixer was primed by flushing a surfactant solution through all inlets to remove air, followed by flushing with adequate DI water to remove the surfactant. The reactants were fed into the mixer with syringe pumps (neMESYS mid-pressure unit with custom SGE glass syringes, Cetoni) and the inert separating stream was fed via a MilliGat LF piston pump (Global FIA). Total flowrate varied from 0.4 to 4.3 ml/min for the experiments. All pumps were controlled via a custom built LabView interface. For temperature control, the mixer and the coil reactor were submerged in a stirred water bath, with heat and magnetic stirring provided by a hot plate (IKAMAG HS7, IKA). A temperature probe was connected to the hotplate for feedback control. The maximum operation temperature was 60 ^{o}C. Temperature uniformity inside the water bath was verified by placing the temperature probe at different locations in the bath.

2.5. Iron Oxide Nanoparticle synthesis

Iron Oxide nanoparticles (IONPs) were produced via co-precipitation of iron chlorides in basic pH induced by the TEAOH solution. In the flow synthesis all samples were collected 5.6-16.6 min (depending on the flowrates) after the first particles were observed at the outlet. The waiting time corresponded to 2x the residence time, allowing the system to reach a steady state. Since both reagent streams were aqueous, DI water was used as a separating stream. Fouling was monitored by focusing a USB microscope (VEHO Discovery 400) directly on the confluence point.

When nanoparticles were prepared in batch, the iron precursor solution was added into the base solution as rapidly as possible via a pipette under constant stirring. Batches were loaded in rapidly stirred (700 rpm) flat bottom glass vials and never exceeded 5 ml in total volume to minimize inconsistencies in mixing conditions.

2.6. Nanoparticle characterisation

The nanoparticles were characterised with dynamic light scattering (DLS) (Delsa Max Pro, Beckman Coulter) immediately after collection unless stated otherwise. For DLS, measurements were performed with 1/20 dilution of collected samples to avoid multiparticle scattering. Particle size and particle size distribution were obtained with image analysis (ImageJ) using data from a transmission electron microscope (TEM) at 120 kV acceleration voltage (JEOL 1200 EX). For TEM analysis, the samples were magnetically decanted (assisted by adding a small amount of NaCl (~10 mg/mL)) and washed with DI water before being re-dispersed in DI water via ultrasonication (5-20 min depending on the sample) and pipetted on a carbon coated copper grid (400 μm lattice). For X-ray diffraction (XRD) analysis particles washed, magnetically decanted and dried under air. The XRD pattern was acquired with an X-ray diffractometer (PanAlytical X'Pert Pro, Malvern) with Co Kα radiation (λ = 1.789 Å).

3. Results and discussion

3.1. Millifluidic triple stream 3D flow focusing mixer design and characterisation

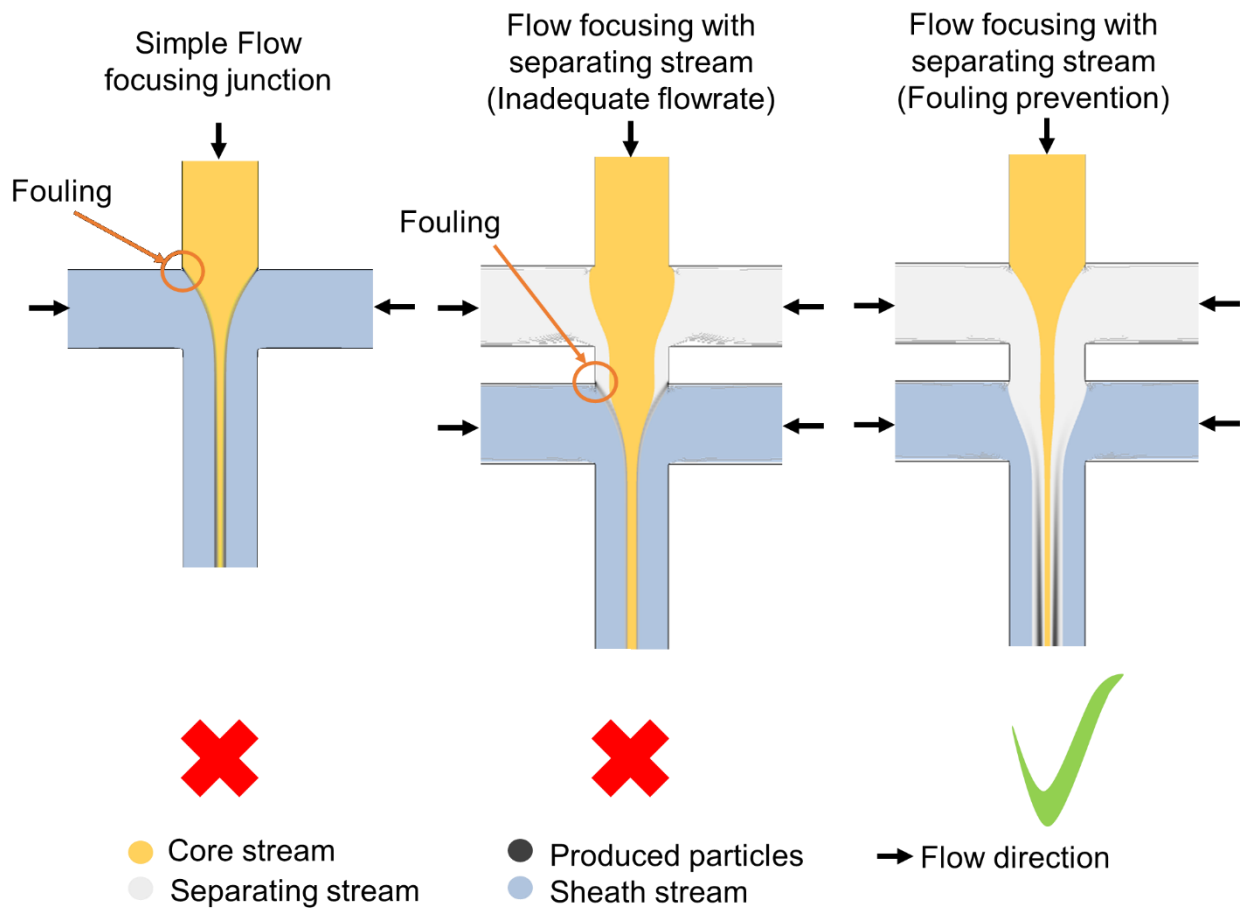

Figure 1: Illustration of fouling in flow focusing junctions during precipitation reaction of the core and the sheath stream. Left) potential fouling position in a simple flow focusing junction, middle) potential fouling positions in a triple stream flow focusing junction when operated with inadequate separating stream, right) fouling prevention in a triple flow focusing junction with adequate separation of the reactant streams.

The concept behind the fouling free operation of the triple stream 3D flow focusing mixer is illustrated in Figure 1. As opposed to the conventional 2 stream flow focusing design where the reaction starts immediately at the confluence point leading to fouling on the wall where the reactants meet (Figure 1, left), in the Triple Stream Flow Focusing Reactor the reactants have to diffuse through a separating stream to react. Considering that the core stream reagents start

diffusing into the separating stream as soon as the streams come in contact, the separating stream has to provide an adequate diffusion barrier to prevent the reactants from the core and sheath stream to meet at the wall. If the core stream reactant diffuses into the separating stream and reaches the wall, the reaction occurs at the edge of the junction where the sheath and the separating stream come in contact (Figure 1, middle), as if no separating stream existed. Increasing the flowrate of the separation stream effectively increases its width[30,39] providing a larger diffusion barrier and shortening the separating and core stream contact time between the two flow focusing junctions, thus effectively preventing fouling (Figure 1, right).

The aim is for the separating stream to shield the walls against fouling, with minimal interference in the reaction. However, having a diffusion barrier between the reactants results in delayed mixing and amplification of concentration gradients, inherent of a laminar flow mixer, which result in an inhomogeneous reaction environment that could potentially affect the product quality. While this issue is to a large extent compensated by the small channel diameters of the millifluidic device (especially after the mixing junctions), minimizing the amount of the separating stream remains an important consideration to further reduce any negative impact and prevent overdilution of the final product.

The minimum separating stream flowrate for fouling prevention depends on the transport properties of the core stream reactant molecules, the relative flowrates of the core and separating stream and the stream contact time between the two flow focusing junctions. One effective way to minimize the separating stream flowrate is by decreasing the distance between the junctions which is more effectively achieved by using a custom chip geometry. The separating stream flowrate can be further reduced by manipulating its own physiochemical properties, such as using a more viscous fluid which would act as a more effective diffusion barrier (e.g. using a glycerol-water mixture as separating stream in a system with aqueous reactants).

It is important to note that while Figure 1 presents a planar 2D geometry, both flow focusing junctions have to isolate the core flow from all directions (like a co-axial flow), so that particles produced do not contact the top and bottom wall of the flow channel, as this would result in a thin line of fouling on them (see Figure S2 in SI).

3.2. Effect of channel height ratio on the flow focusing pattern via CFD simulations

Producing a 3D focusing flow pattern to prevent fouling on the top and bottom of the channel, with an easy to manufacture planar chip device presents a challenge by itself. The 3D effect was produced by tuning the height of the core (H_C), sheath (H_{Sh}) and main (H_M) flow channels (Figure

2 left) and CFD simulations were used to identify the optimal ratios of these channel heights. The simulated domain comprised of the flow focusing junction of the mixer and the channel leading to the outlet. Simple cross-shaped flow focusing junction geometries were used to establish the channel height ratio that results in 3D flow focusing patterns (Figure 2 left). The geometric parameters of the various flow focusing junctions are summarized in Table 1. In a later stage, a geometry with an additional lateral channel was used to simulate the separating stream. All 3D domains exhibit double planar symmetry and thus only a quarter of each was included in the model, significantly saving computational time.

Since the flow focusing behavior was expected to depend mostly on the parabolic velocity profile of the lateral sheath stream and the core/sheath flowrate ratio, simulations for every geometry were run for the same sheath stream Reynolds number (calculated as described in the SI, section 2.1) and for a constant core/sheath flowrate ratio Q_C/Q_{Sh}= 1/10. The chosen flowrate ratio aids to help visualization. A range of Reynolds numbers between 1 and 50 was examined, as it encompasses the inertial laminar flow regime which is of interest in this work.

Table 1: Summary of geometric parameters of the 3D flow focusing junction used in the simulations (see Fig 2)

Geometry	W (mm)	H_M (mm)	H_{Sh} (mm)	H_C (mm)
A	1	1.5	1.5	1
B	1	2	2	1
C	1	3	3	1
D	1	2	3	1
E	1	1	3	1
F	1	1	2	1

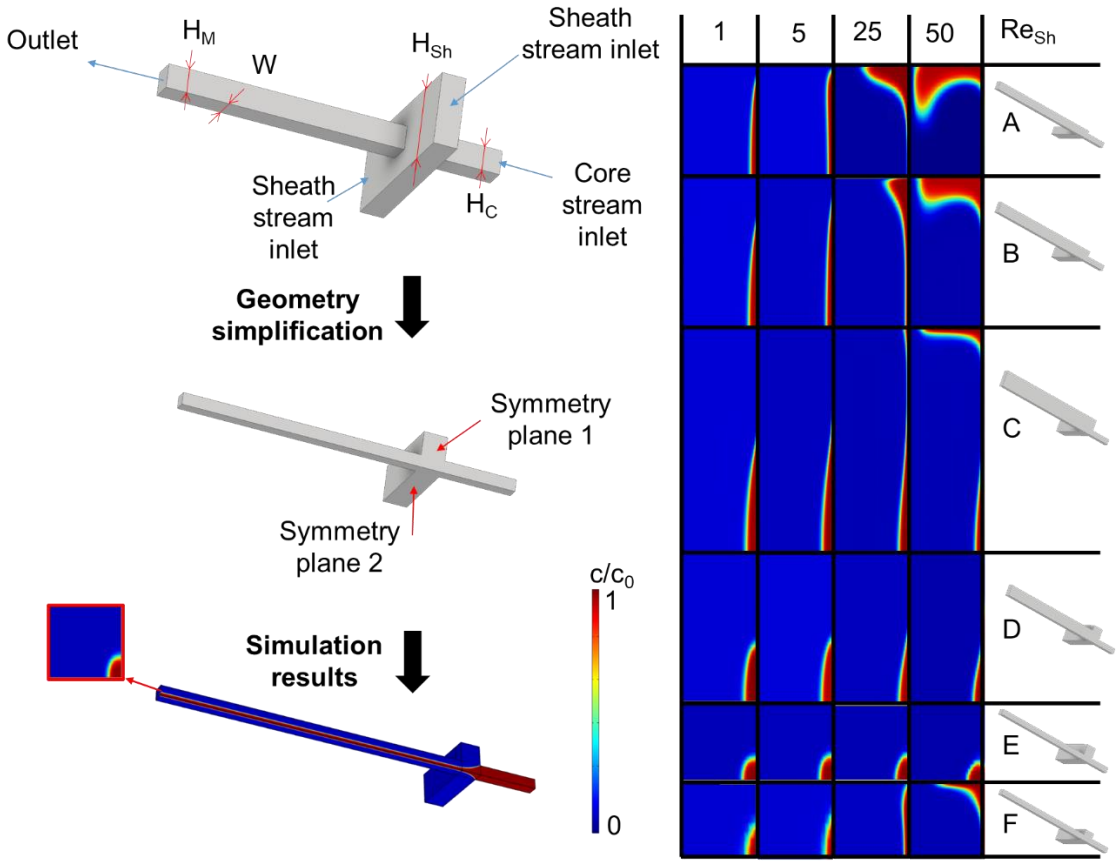

Figure 2: Summary of CFD simulations. (Left) Simulation domain simplification and simulation results presentation. A non-diffusive tracer enters the system at concentration $c/c_0 = 1$ (depicted with red colour) at the core inlet and follows the streamlines. The concentration map obtained at the outlet is representative of the flow pattern. (Right) Concentration map obtained at the outlet of the simulated domain for different geometries and for sheath stream Reynolds number (Re_{Sh}) 1-50.

The resulting flow patterns for all the tested geometries are represented in Figure 2 (Right) as concentration maps of a non-diffusive tracer entering via the core inlet. The maximum concentration of the tracer is depicted with a red colour and zero concentration with a blue colour. Intermediate concentration values seen around the patterns as yellow/green, are a result of numerical diffusion. With the chosen meshing strategy, numerical diffusion does not significantly affect the obtained concentration maps (refer to SI, section 2). While all the tested geometries provide a 3D focusing effect of the core stream for low Reynolds numbers, as the flowrate increases so does the irregularity of the flow pattern. The “butterfly shaped” concentration maps obtained for high Reynolds numbers can be attributed to the parabolic velocity profile of the lateral

streams, which is characteristic of the laminar flow. Higher velocity fluid in the middle of the lateral channel pushes the fluid of the core stream towards the top and bottom channels where the velocity of the lateral stream is lower. Similar flow patterns have been observed for simple cross shaped flow focusing geometries and verified via confocal microscopy[39,47]. Increasing the H_{Sh}/H_C ratio while keeping $H_{Sh} = H_M$, as in geometries A, B and C, reduces the amount of core stream pushed towards the walls at high Re, as the velocity gradient of the sheath stream at the confluence point with the core stream becomes smaller. The flow pattern is drastically altered by reducing the H_M/H_{Sh} ratio, as in geometries D and E. The additional confinement forces the sheath fluid to move towards the core fluid from every direction, leading to flow patterns resembling those obtained by co-axial geometries. However, this effect still depends on the H_{Sh}/H_C ratio, as shown in the pattern obtained for geometry F, which indicates that adjusting both H_{Sh}/H_C and H_M/H_{Sh} channel height ratios is equally important to achieve the desired flow pattern for the operational range of flowrates.

3.3. Triple stream 3D flow focusing mixer design and flow pattern evaluation

The final design of the flow focusing reactor was based on the simulation results. Geometry E was chosen as the most appropriate to produce the desired flow pattern. In addition to the uniform sheathing of the core stream in almost the whole Reynolds range investigated, the fact that $H_M = H_C$ makes it easier to implement multiple consecutive flow focusing junctions to accommodate the separating stream without the need of further adjusting the geometry of each junction. In addition to the simulation results, the design was also subject to constraints related to the choice of milling as the manufacturing process. This defined the minimum channel width of 0.6 mm that was used, and the distance between the two flow focusing junctions which was set as 0.3 mm to allow enough material between the lateral channels for the bonding process. The fluid domain for the final design and a schematic of how this 3D domain was translated into a planar chip geometry are presented in Figure 3.

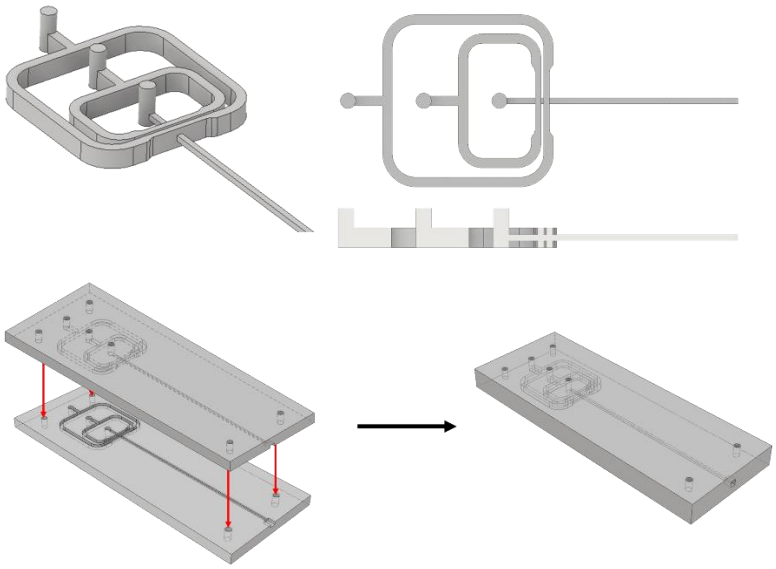

Figure 3: Millifluidic triple stream 3D flow focusing mixer design based on geometry E of Fig. 2. (Top) Complete flow domain based on simulation results including a 3D isometric view, a top view and a cross-sectional side view. (Bottom) Schematic of patterns engraved in two PMMA layers bonded together to form a closed channel device with three inlets on the top and an outlet in the direction of the flow channel.

The hydrodynamic behavior of the manufactured mixer is presented in Figure 4. Blue dye was introduced in the separating stream as a simple means of visualizing all 3 layers. DI water was introduced in the core and outer sheath stream. With this setup the separating stream appears as a blue annulus that engulfs the core stream and is surrounded by the outer sheath stream. Flow focusing was observed both at the chip mixer (Figure 4 A) and at the outlet capillary connected to it (Figure 4 B), indicating that the flow pattern was mostly undisturbed after exiting the mixer if the capillary was straight. The flow pattern in the capillary was also observed from the side (Figure 4 C), proving that 3D flow focusing has been achieved successfully. The height of the focused stream (Figure 4 C) is slightly higher than its width (Figure 4 B) indicating an oval cross section of the focused stream which agrees with the corresponding simulation results for the device that also produces a similarly shaped flow pattern (Figure 4 D and E). The conditions depicted in Figure 4 are similar to those used in the IONP synthesis.

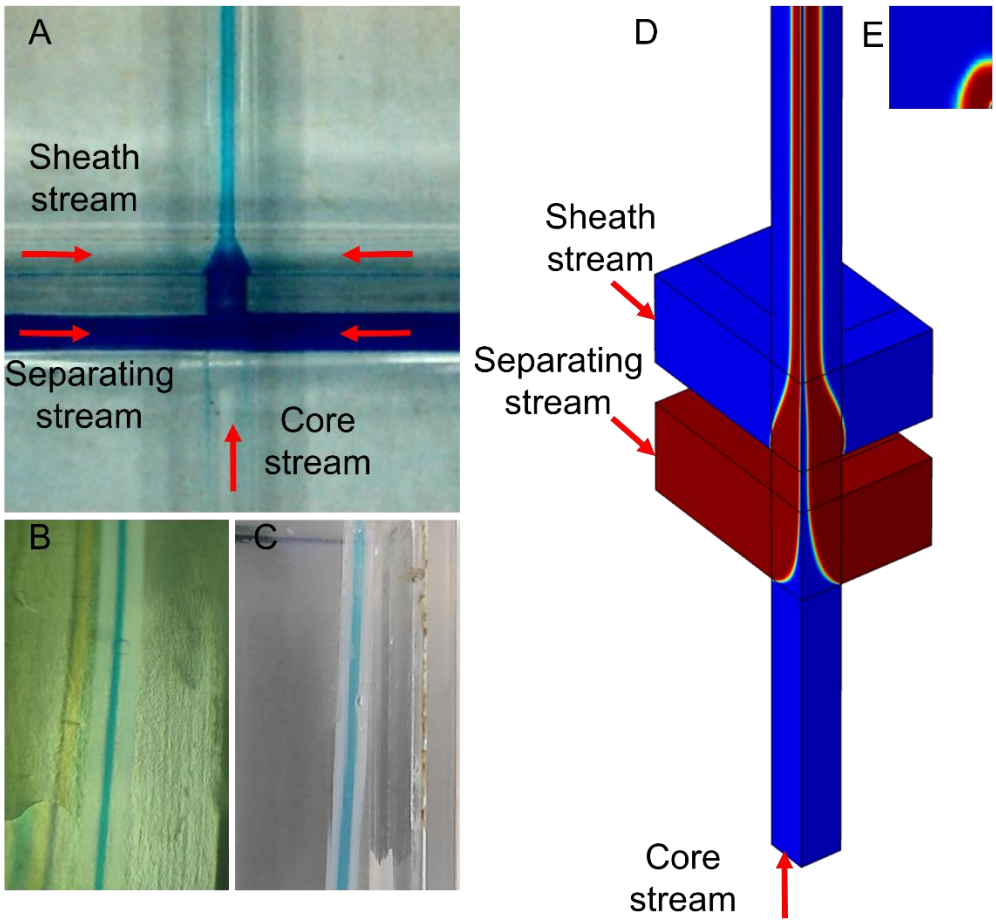

Figure 4: Visualisation of the separating stream: A) Demonstration of 3D flow focusing in the triple stream 3D flow focusing mixer, B) top view of the capillary after the mixer, C) side view of the capillary after the mixer, D) isometric view of a simulated device (same dimensions with the real device) with a non diffusive tracer (red colour) introduced in the separating stream, for the same flow conditions as the real device. The concentration map represents the flow pattern in the simulated device while the red arrows indicate the inlets of the simulated geometry. E) cross section at the outlet of the simulated domain. The flow conditions depicted are similar to those used in the nanoparticle synthesis. Core stream: 0.1 ml/min, separating stream: 0.3 ml/min, sheath stream: 1 ml/min.

3.4. Non-fouling millifluidic Iron oxide nanoparticle synthesis

3.4.1. Translation from batch to a continuous millifluidic process

The flow focusing reactor was used for IONP synthesis via co-precipitation of iron precursor by TEAOH. In preliminary batch experiments, various stages of the synthesis were observed over time: particles formed immediately after the mixing of the reactants and agglomerated within few seconds into flake-like structures. These large agglomerates remained visible over a ~20 min period, while breaking under the effect of TEA^+ before finally forming a colloidal solution of nanoparticles. The same process stages were observed in a typical millifluidic synthesis along the reactor. The initial mixing took place in the designed chip mixer, where the iron precursor was introduced in the core stream, the TEAOH solution in the outer sheath, and both reactants were separated by an inert DI water stream. The initial particle formation took place in the chip mixer shortly after the two reactants met by diffusing through the separating stream. The particles remained in the separating stream where they had initially formed, flowing out of the mixer chip. Agglomeration started in the capillary connected to the chip and was observed as breaking of the flow focusing pattern into segments that formed the flake structures which deagglomerated while traveling along the capillary coil, forming a colloidal solution that was collected at the reactor outlet. Videos of the various stages of the millifluidic synthesis can be found in the SI, section 4.

3.4.2. Non-fouling operation of the triple stream 3D flow focusing mixer

The chip device presented in sections 3.1-3.3 controls the initial mixing of the reactants and prevents wall particle contact which could lead to fouling at the confluence point and disrupt the process. The first step for employing the flow focusing device for nanoparticle production was to identify the minimum flowrate of separating stream for non-fouling operation. The minimum separating stream flowrate was identified experimentally, by observing the flow focusing junction with the microscope to seek out any occurrence of fouling (see SI, section 5), for a range of core stream (iron precursor) flowrates between 0.02 ml/min (minimum pulsation free flowrate achieved with the syringe pump) and 1 ml/min. It was found that for the flowrate range examined, the required separating stream flowrate rises proportionally to the iron precursor flowrate indicating that a specific ratio is required which is suitable to the system properties (fluid transport properties and geometry). However, it is speculated that for very low total flowrates (core stream and separating stream), fouling will occur for any ratio as radial diffusion becomes dominant over axial convection. The operation range of the triple stream 3D flow focusing device could be extended to lower flowrates by using a different fluid as separating stream or reducing the distance between

the two flow focusing junctions with more advanced manufacturing methods. Figure 5 shows the operation range where the device was used for iron oxide nanoparticle production without fouling. It was found that the flowrate of the sheath stream containing the base had negligible effect on the curve in Figure 5 when tested for the flowrates of interest (0.1 – 2 ml/min of sheath stream).

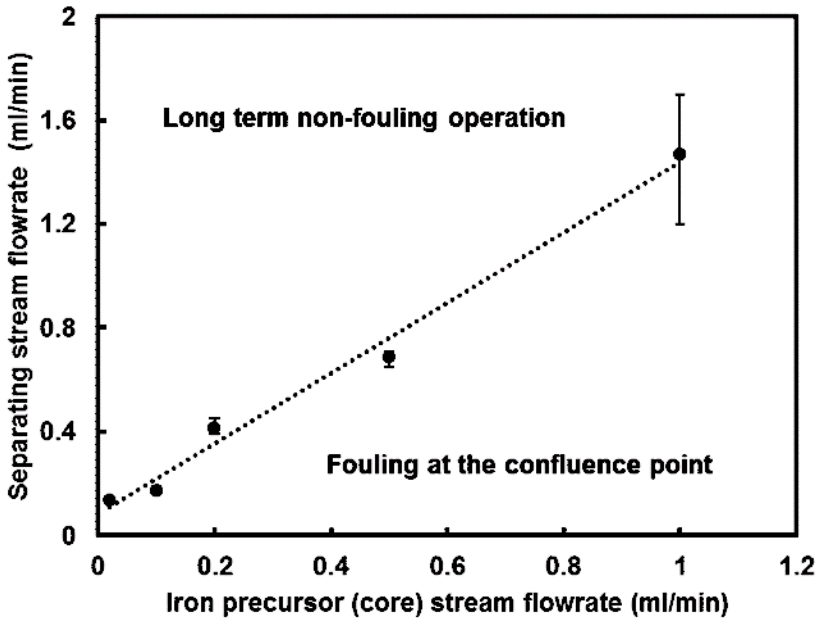

Figure 5: Operation map for non-fouling operation of the triple stream 3D flow focusing mixer for room temperature production of IONPs. Above the curve the device can operate without fouling for long periods of time, while below fouling was observed at the confluence point.

Appealing as a room temperature synthesis may be, literature suggests that increasing the temperature is expected to produce significantly better results in terms of particle quality due to faster formation of magnetite as the dominant phase[17,48]. However, an additional effect of increased temperature is the acceleration of mass transfer by increasing the diffusion coefficients of solute species. This effect holds true for all types of mixers at the lowest scale of homogenization (micromixing) where diffusion is the dominant mechanism, and is even more important in laminar flow mixers, such as the one investigated in this work, where diffusion is the only mixing mechanism[49]. Thus, for non-fouling operation, it is expected that an increased amount of separating stream would be required to counteract the enhanced diffusion of iron ions towards the wall. It was found that for 0.1 mL/min of iron precursor solution, a rise of temperature to 60 ^{o}C

increased the demand for separating stream from 0.18 mL/min to slightly less than 0.6 mL/min, verifying the assumption.

3.4.3. Assessment of the triple stream 3D flow focusing reactor system behavior and particle quality

While the initial precipitation handled by the triple stream flow focusing mixer is the most fouling-prone stage of the IONP synthesis, one cannot overlook the importance of what happens downstream the chip mixer. During the agglomeration stage that takes place downstream of the chip, fouling could still occur. Preliminary experiments with 1:1 flowrate ratio for the iron precursor and base streams (the direct adaptation of the batch synthesis in terms of reactant volumes) showed that a portion of the agglomerates was attaching on the wall in the capillary section after the mixer and thus, a way to prevent fouling after the chip was still required. Based on preliminary batch experiments showing that deagglomeration is greatly accelerated (the flake-like agglomerates disappeared within few minutes) by increasing the base:iron precursor volume ratio, the reactant flowrate ratio in the millifluidic synthesis was adapted accordingly. In addition, in the laminar flow environment of the mixer increasing the ratio of the sheath (base) to core (iron precursor) streams was expected to further accelerate mixing by reducing the core diffusion distance and further confine particles forming in the core stream. To evaluate the effect of the adjusted millifluidic synthesis on the overall hydrodynamic behavior and particle quality, the reactor was operated with different concentrations of the base stream and varying flowrate ratios. Table 2 summarizes the experiments performed for this purpose. In all cases, the conditions were chosen to avoid fouling in the triple stream flow focusing mixer section, as discussed in section 3.4.2.

Table 2: Summary of the operating conditions used for the IONP synthesis experiments using the triple stream 3D flow focusing reactor. $Q_{TEAOH}/Q_{Fe^{x+}}$ = Base : iron precursor flowrate ratio, $Q_{sep}/Q_{Fe^{x+}}$ = separating stream: iron precursor flowrate ratio, $[TEAOH]$ = base stream concentration. The iron precursor flowrate was $Q_{Fe^{x+}}$ = 0.1 ml/min with a total iron concentration of 0.1 M. The residence time was based on the capillary coil volume (the volume of the flow focusing mixer was negligible) and the total flowrate.

Experiment /Sample	$\frac{Q_{TEAOH}}{Q_{Fe^{x+}}}$	$\frac{\mathrm{Q_{sep}}}{\mathrm{Q_{Fe^{x+}}}}$	$[TEAOH]$ (M)	T (°C)	Residence time (min)	Fouling after the mixer chip
1	10	2	0.570	20	9.30	None
2	10	4	0.570	20	8.06	None
3	10	7	0.570	20	6.72	None
4	10	2	0.114	20	9.30	Minor
5	10	4	0.114	20	8.06	Minor
6	10	7	0.114	20	6.72	Minor
7	10	2	0.057	20	9.30	Minor
8	10	4	0.057	20	8.06	Minor
9	10	7	0.057	20	6.72	Minor
10	20	2	0.570	20	5.26	None
11	40	2	0.570	20	2.81	None
12	1	2	0.570	20	30.24	Major
13	1	6	0.570	60	15.12	Major
14	10	6	0.570	60	7.11	None
15	20	6	0.570	60	4.48	None

System wide non-fouling behavior was obtained in all cases with the maximum flowrate and maximum concentration of base (experiments 1-3,10,11,14,15) due to the accelerated redispersion of agglomerated NPs under the effect of TEA^+. For $Q_{sep}/Q_{Fe^{x+}}$ = 2, and $[\mathrm{TEAOH}]$ = 0.57 M, the reactor was operated for 4 consecutive 1.5 h runs, stopping only to refill the syringe pumps, without cleaning in between and without signs of fouling appearing at any part of the mixer or the coupled capillary coil. For lower base concentrations as in experiments 4, 5 and 6 a thin line of particle deposition emerged at the capillary after the mixer becoming clearly visible after 10 min of operation. In experiments 7, 8 and 9, the result was similar,

but deposition happened shortly after the experiment started. In experiments 10 and 11 which aimed to improve the mixing by increasing the sheath:core flowrate ratio, no particle flakes were observed and no fouling seemed to occur along the reactor. However, in the collected samples only a non-magnetic pale yellow sediment was present. The yellow sediment likely consisted of iron hydroxides or oxyhydroxides, produced as a result of the initial nucleation taking place at a very high pH value[50]. At 60 ^{o}C, the hydrodynamic behavior was similar to what was observed at room temperature. Equal reactant flowrates in experiment 13 led to fouling downstream the mixer, while in experiment 14 the reactor was operated without any signs of fouling for several 1.5 h windows. Finally, experiment 15 also led to non-fouling operation with magnetically separable product. In that case however the supernatant was not clear, possibly indicating incomplete reaction due to short residence time.

In all cases where fouling was observed, it occurred in the short capillary section connecting the chip mixer with the capillary coil. No fouling was observed in the capillary coil, which indicates the onset of particle stabilization that prevents attractive interactions between the wall and the particles happens at the beginning of the coil section. In addition, secondary Dean flows induced by the coil, potentially promote the dispersion of the flake like agglomerates and prevent their sedimentation, thus aiding deagglomeration. Photos of fouling occurrence at the capillary after the flow focusing mixer section can be found in the SI section 6.

The particle quality was evaluated via XRD and TEM. For all room temperature experiments, although XRD confirmed the presence of magnetite, TEM analysis revealed that a secondary solid phase was also produced, which appeared as a lighter colored matrix that engulfed the primary 8 nm particles (Figure 6a). The secondary phase likely consisted of iron hydroxides/oxyhydroxides that have been reported to arise in laminar flow conditions[51]. In highly basic conditions (such as in cases 1-3) the secondary phase possibly evolves into the yellow sediments observed within 48 h after sample collection, leaving a dark brown dispersion of magnetite/maghemite nanoparticles in the supernatant. At 60 ^{o}C, only magnetite/maghemite nanoparticles were produced (shown in Figure 6b for case 14), as verified by XRD, which can be attributed to elevated temperature simultaneously accelerating mixing via diffusion and promoting evolution of intermediate species to magnetite[48], demonstrating the superiority of the elevated temperature synthesis of IONPs.

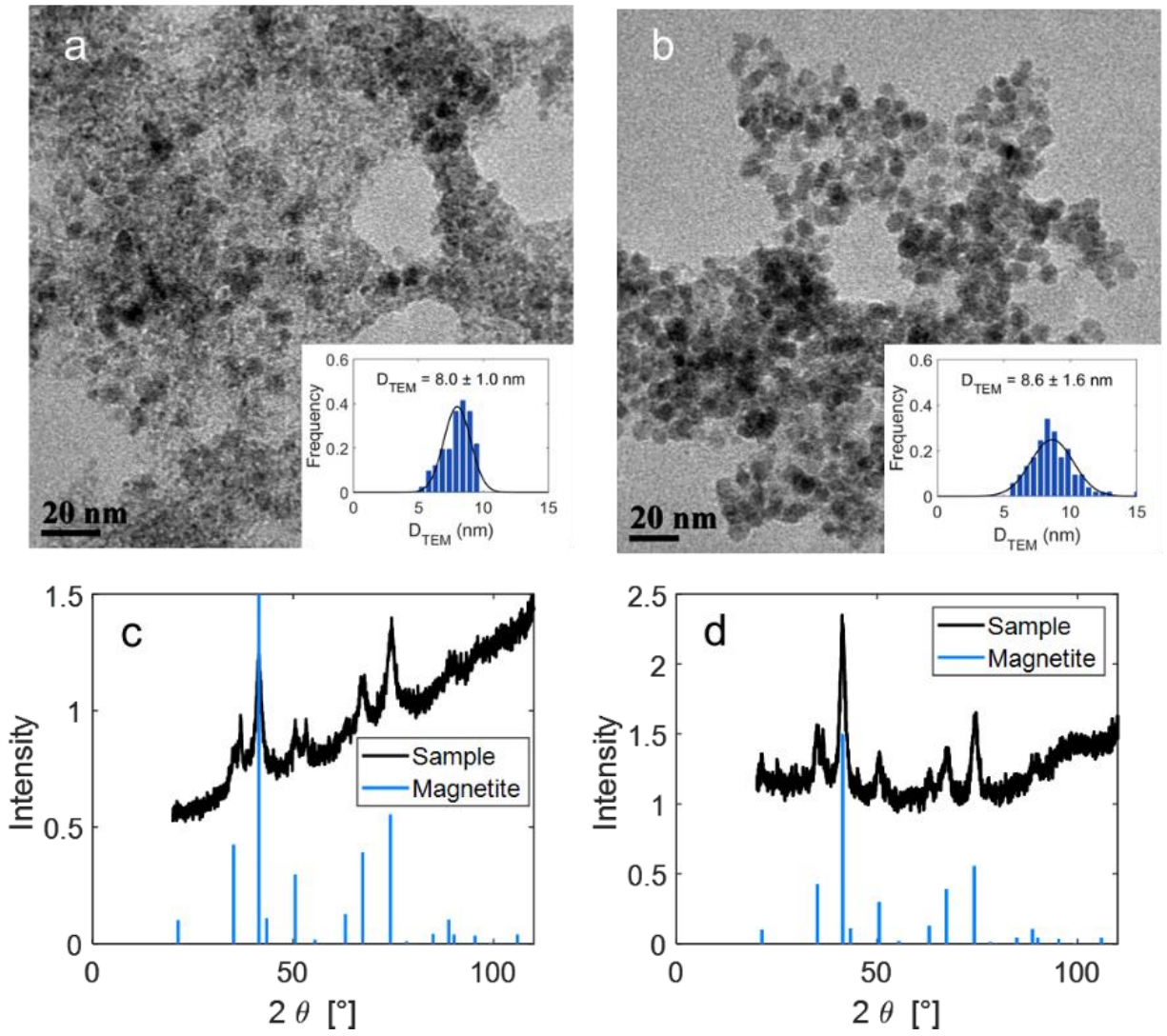

Figure 6: Characterisation of IONPs produced with the triple stream 3D flow focusing reactor. a) TEM image of sample 1, b) TEM image of sample 14. Both TEM images contain histograms with the particle size distribution. c) XRD spectrum of sample 1, d) XRD spectrum of sample 14. For experimental conditions see Table 2.

IONPs produced with the flow focusing reactor that were magnetically decanted and redispersed in water shortly after collection, exhibited excellent colloidal stability for days afterwards without any additives (with the exception of experiments 10-13). DLS analysis for samples 1-9 directly after collection showed that the hydrodynamic diameters of the particles were in the range 40-170 nm, indicating that each particle is a stabilized nanosied agglomerate of smaller particles. While no clear relationship was found between reactor hydrodynamics and the final colloidal

stability, DLS analysis of the particle dispersions obtained from experiments 1-9 directly after collection was used as means of assessing the particle stabilisation with the assumption that faster or more effective stabilization would break-up the initially formed agglomerates more efficiently leading to smaller particles. The following trends were observed: in experiments 1-3, the hydrodynamic diameter increased with increasing separating stream flowrate, indicating that the stabilisation of the particles is dependent on the initial mixing conditions, with slower mixing allowing larger agglomerates to form before stabilisation starts. A similar trend was seen for experiments 4-9, but cannot be considered as conclusive since the size slightly decreased over the course of the following 30 min, indicating that particle stabilisation was not complete inside the reactor. Further investigating cases 4-6, it was found that after the sample was collected, further mixing (e.g., by collecting the sample in a stirred vessel) had little effect on the evolution of deagglomeration. The second trend observed for experiments 1-9 is that for a given residence time inside the reactor, higher base (and thus TEA^+) concentration, gives smaller particles by accelerating the initial deagglomeration step.

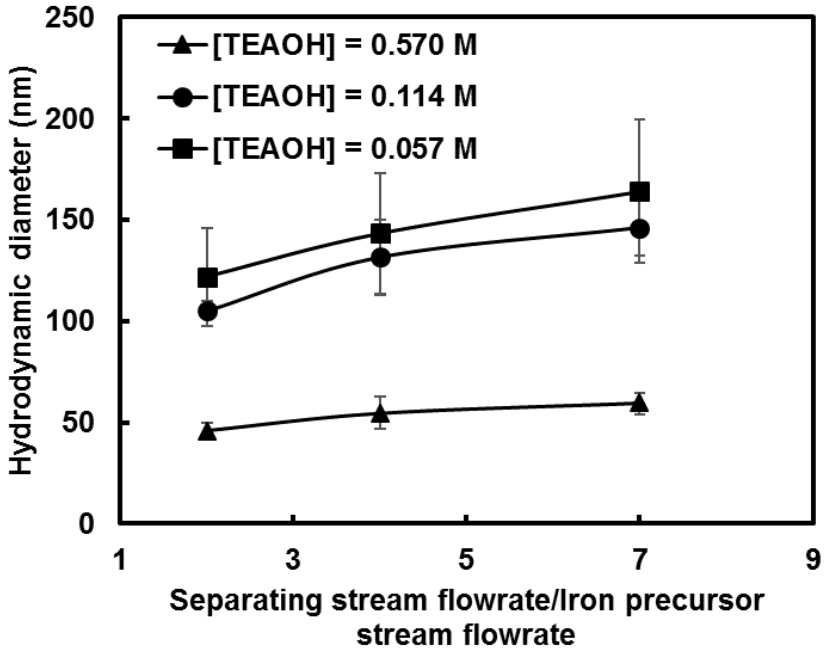

Figure 7: DLS analysis of samples 1-9, showing aggregate size variation with separating stream flowrate/iron precursor stream flowrate ratio and TEAOH concentration.

4. Conclusions

This work presented the design of a millifluidic reactor that was able to continuously produce magnetite/maghemite nanoparticles via rapid co-precipitation for long time time periods, utilising a combination of multiple flow focusing and fast particle deagglomeration by taking advantage of the stabilizing effect of excess TEAOH, to simultaneously prevent two different fouling mechanisms in the reactor system. A novel millifluidic mixer was designed to prevent fouling by confining the reactive flow via 3D flow focusing, and by introducing a separating stream to prevent premature reaction and fouling at the mixing point where the initial nucleation step takes place. Informed by CFD simulations, the classic cross-shaped flow focusing junction was adapted to enable a 3D flow focusing pattern similar to co-axial configurations for a wide sheath stream Reynolds number window within the laminar flow regime, by identifying the optimal height ratios of the core stream, lateral and main (outlet) channels. Especially important was the reduction of the main channel height compared to the lateral one, as it introduced an additional confinement effect, critical for achieving a coaxial-like flow pattern in a planar device. The chosen 3D flow focusing geometry allowed the incorporation of two sequential 3D cross shaped junctions in a very small footprint (with a distance of 300 μm between them) that facilitated the use of a separating stream to prevent particle formation from happening at the confluence point of the reactant streams, which otherwise took place due to rapid precipitation of particles.

Fouling prevention downstream the triple stream 3D flow focusing mixer was also addressed, since it is not always practical to maintain a straight flow focusing channel that prevents particle wall interactions, especially when long residence times or heating is a requirement for the reactions taking place. Thus, the IONP co-precipitation reaction used for demonstrating the effectiveness of the mixer was optimised, so as to avoid fouling throughout the following deagglomeration/stabilization step that took place in a millifluidic capillary coil following the flow focusing mixer. Fouling throughout the coil was prevented using concentrated TEAOH, which accelerated the stabilisation of produced particles and prevented their sedimentation. At room temperature, the high pH value (due to the concentrated base) gave rise to nonmagnetic by-products which required an additional aging step to separate the magnetic IONP colloidal solution. At 60 ^{o}C magnetic particles were obtained without need for byproduct separation and were of superior quality. The importance of the designed triple stream 3D flow focusing device should not be overshadowed by the fast stabilization described above, since fouling at the mixer did occur even at high base concentrations, because of the difference between the initial precipitation and the stabilization kinetics.

The reported approach may be of more general appeal in particle synthesis. The designed mixer, offering fouling prevention due to hydrodynamics can potentially find use in other solid producing systems that suffer from fouling. In addition, since the design can operate in a wide range of Reynolds numbers in the laminar flow regime, it can enable the use of sub-100 μm-scale mixers based on the same principles that would allow even higher mass transfer rates when these are required. Finally, the ease and reproducibility of manufacturing may further enhance the applicability of the design.

Supplementary material

The following are available: 1. Preliminary experiments showing fouling in simple flow focusing configurations. 2. Simulation details of 3D flow focusing geometry. 3. Reactor manufacturing details. 4. Videos of nanoparticle synthesis in the 3D flow focusing reactor assembly. 5. Fouling in the triple stream 3D flow focusing mixer. 6. Fouling after the triple stream 3D flow focusing mixer.

Acknowledgements

We thank the EPSRC (EP/M015157/1) through the Manufacturing Advanced Functional Materials (MAFuMa) scheme for financial support. Georgios Gkogkos is grateful to the Hugh Walter Stern PhD studentship for his funding.

References

1. Sebastian, V., Khan, S. A. & Kulkarni, A. A. Perspective article: Flow synthesis of functional materials. *J. Flow Chem.* **7**, 96–105 (2017).

2. Sebastian, V., Arruebo, M. & Santamaria, J. Reaction engineering strategies for the production of inorganic nanomaterials. *Small* **10**, 835–853 (2014).

3. Gao, Y., Pinho, B. & Torrente-Murciano, L. Recent progress on the manufacturing of nanoparticles in multi-phase and single-phase flow reactors. *Curr. Opin. Chem. Eng.* **29**, 26–33 (2020).

4. Gonidec, M. & Puigmartí-Luis, J. Continuous-versus segmented-flow microfluidic

synthesis in materials science. *Crystals* **9**, (2019).

5. Schoenitz, M., Grundemann, L., Augustin, W. & Scholl, S. Fouling in microstructured devices: A review. *Chem. Commun.* **51**, 8213–8228 (2015).

6. Hartman, R. L. Managing solids in microreactors for the upstream continuous processing of fine chemicals. *Org. Process Res. Dev.* **16**, 870–887 (2012).

7. Huang, H., Du Toit, H., Panariello, L., Mazzei, L. & Gavriilidis, A. Continuous synthesis of gold nanoparticles in micro- And millifluidic systems. *Phys. Sci. Rev.* **6**, (2021).

8. Xu, Z., Lu, C., Riordon, J., Sinton, D. & Moffitt, M. G. Microfluidic manufacturing of polymeric nanoparticles: Comparing flow control of multiscale structure in single-phase staggered herringbone and two-phase reactors. *Langmuir* **32**, 12781–12789 (2016).

9. He, Y., Kim, K. J. & Chang, C. H. Segmented microfluidic flow reactors for nanomaterial synthesis. *Nanomaterials* **10**, 1–21 (2020).

10. Pan, L. J., Tu, J. W., Ma, H. T., Yang, Y. J., Tian, Z. Q., Pang, D. W. & Zhang, Z. L. Controllable synthesis of nanocrystals in droplet reactors. *Lab Chip* **18**, 41–56 (2018).

11. Chow, E., Raguse, B., Della Gaspera, E., Barrow, S. J., Hong, J., Hubble, L. J., Chai, R., Cooper, J. S. & Sosa Pintos, A. Flow-controlled synthesis of gold nanoparticles in a biphasic system with inline liquid-liquid separation. *React. Chem. Eng.* **5**, 356–366 (2020).

12. Niu, G., Zhang, L., Ruditskiy, A., Wang, L. & Xia, Y. A droplet-reactor system capable of automation for the continuous and scalable production of noble-metal nanocrystals. *Nano Lett.* **18**, 3879–3884 (2018).

13. Baber, R., Mazzei, L., Thanh, N. T. K. & Gavriilidis, A. Synthesis of silver nanoparticles using a microfluidic impinging jet reactor. *J. Flow Chem.* **6**, 268–278 (2016).

14. Sahoo, K. & Kumar, S. Green synthesis of sub 10 nm silver nanoparticles in gram scale using free impinging jet reactor. *Chem. Eng. Process. - Process Intensif.* **165**, 108439 (2021).

15. Geng, H. & Cho, S. K. Lab on a Chip Antifouling digital microfluidics using lubricant infused porous film †. **19**, 2275 (2019).

16. Qin, Y., Yeh, P., Hao, X. & Cao, X. Developing an ultra non-fouling SU-8 and PDMS

hybrid microfluidic device by poly(amidoamine) engraftment. *Colloids Surfaces B Biointerfaces* **127**, 247–255 (2015).

17. Besenhard, M. O., LaGrow, A. P., Hodzic, A., Kriechbaum, M., Panariello, L., Bais, G., Loizou, K., Damilos, S., Margarida Cruz, M., Thanh, N. T. K. & Gavriilidis, A. Co-precipitation synthesis of stable iron oxide nanoparticles with NaOH: New insights and continuous production via flow chemistry. *Chem. Eng. J.* **399**, 125740 (2020).

18. Guerrini, L., Alvarez-Puebla, R. A. & Pazos-Perez, N. Surface modifications of nanoparticles for stability in biological fluids. *Materials (Basel).* **11**, 1–28 (2018).

19. Takagi, M., Maki, T., Miyahara, M. & Mae, K. Production of titania nanoparticles by using a new microreactor assembled with same axle dual pipe. *Chem. Eng. J.* **101**, 269–276 (2004).

20. Génot, V., Desportes, S., Croushore, C., Lefèvre, J. P., Pansu, R. B., Delaire, J. A. & von Rohr, P. R. Synthesis of organic nanoparticles in a 3D flow focusing microreactor. *Chem. Eng. J.* **161**, 234–239 (2010).

21. Lu, M., Ozcelik, A., Grigsby, C. L., Zhao, Y., Guo, F., Leong, K. W. & Huang, T. J. Microfluidic hydrodynamic focusing for synthesis of nanomaterials. *Nano Today* **11**, 778–792 (2016).

22. Zhang, L., Wang, Y., Tong, L. & Xia, Y. Synthesis of colloidal metal nanocrystals in droplet reactors: The pros and cons of interfacial adsorption. *Nano Lett.* **14**, 4189–4194 (2014).

23. Abou-Hassan, A., Neveu, S., Dupuis, V. & Cabuil, V. Synthesis of cobalt ferrite nanoparticles in continuous-flow microreactors. *RSC Adv.* **2**, 11263–11266 (2012).

24. Bemetz, J., Wegemann, A., Saatchi, K., Haase, A., Häfeli, U. O., Niessner, R., Gleich, B. & Seidel, M. Microfluidic-based synthesis of magnetic nanoparticles coupled with miniaturized NMR for online relaxation studies. *Anal. Chem.* **90**, 9975–9982 (2018).

25. Rhee, M., Valencia, P. M., Rodriguez, M. I., Langer, R., Farokhzad, O. C. & Karnik, R. Synthesis of size-tunable polymeric nanoparticles enabled by 3D hydrodynamic flow focusing in single-layer microchannels. *Adv. Mater.* **23**, 79–83 (2011).

26. Baby, T., Liu, Y., Middelberg, A. P. J. & Zhao, C. X. Fundamental studies on throughput capacities of hydrodynamic flow-focusing microfluidics for producing monodisperse

polymer nanoparticles. *Chem. Eng. Sci.* **169**, 128–139 (2017).

27. Baber, R., Mazzei, L., Thanh, N. T. K. & Gavriilidis, A. Synthesis of silver nanoparticles in a microfluidic coaxial flow reactor. *RSC Adv.* **5**, 95585–95591 (2015).

28. Abou Hassan, A., Sandre, O., Cabuil, V. & Tabeling, P. Synthesis of iron oxide nanoparticles in a microfluidic device: Preliminary results in a coaxial flow millichannel. *Chem. Commun.* 1783–1785 (2008).

29. Norfolk, L., Rawlings, A. E., Bramble, J. P., Ward, K., Francis, N., Waller, R., Bailey, A. & Staniland, S. S. Macrofluidic coaxial flow platforms to produce tunable magnetite nanoparticles: A study of the effect of reaction conditions and biomineralisation protein mms6. *Nanomaterials* **9**, (2019).

30. Knight, J. B., Vishwanath, A., Brody, J. P. & Austin, R. H. Hydrodynamic focusing on a silicon chip: Mixing nanoliters in microseconds. *Phys. Rev. Lett.* **80**, 3863–3866 (1998).

31. Yaghmur, A., Ghazal, A., Ghazal, R., Dimaki, M. & Svendsen, W. E. A hydrodynamic flow focusing microfluidic device for the continuous production of hexosomes based on docosahexaenoic acid monoglyceride †. *Phys. Chem. Chem. Phys* **21**, 13005 (2019).

32. Lim, J. M., Bertrand, N., Valencia, P. M., Rhee, M., Langer, R., Jon, S., Farokhzad, O. C. & Karnik, R. Parallel microfluidic synthesis of size-tunable polymeric nanoparticles using 3D flow focusing towards in vivo study. *Nanomedicine Nanotechnology, Biol. Med.* **10**, 401–409 (2014).

33. Baber, R., Mazzei, L., Thanh, N. T. K. & Gavriilidis, A. An engineering approach to synthesis of gold and silver nanoparticles by controlling hydrodynamics and mixing based on a coaxial flow reactor. *Nanoscale* **9**, 14149–14161 (2017).

34. Abou Hassan, A., Sandre, O., Cabuil, V. & Tabeling, P. Synthesis of iron oxide nanoparticles in a microfluidic device: Preliminary results in a coaxial flow millichannel. *Chem. Commun.* 1783–1785 (2008).

35. Abou-Hassan, A., Sandre, O., Neveu, S. & Cabuil, V. Synthesis of goethite by separation of the nucleation and growth processesof ferrihydrite nanoparticles using microfluidics. *Angew. Chemie - Int. Ed.* **48**, 2342–2345 (2009).

36. Wang, Y. & Seidel, M. Strategy for fast manufacturing of 3D hydrodynamic focusing multilayer microfluidic chips and its application for flow-based synthesis of gold

nanoparticles. *Microfluid. Nanofluidics* **25**, 64 (2021).

37. Erfle, P., Riewe, J., Bunjes, H. & Dietzel, A. Goodbye fouling: A unique coaxial lamination mixer (CLM) enabled by two-photon polymerization for the stable production of monodisperse drug carrier nanoparticles. *Lab Chip* **21**, 2178–2193 (2021).

38. Nagasawa, H. & Mae, K. Development of a new microreactor based on annular microsegments for fine particle production. *Ind. Eng. Chem. Res.* **45**, 2179–2186 (2006).

39. Park, H. Y., Qiu, X., Rhoades, E., Korlach, J., Kwok, L. W., Zipfel, W. R., Webb, W. W. & Pollack, L. Achieving uniform mixing in a microfluidic device: Hydrodynamic focusing prior to mixing. *Anal. Chem.* **78**, 4465–4473 (2006).

40. Rodriguez-Trujillo, R., Kim-Im, Y. H. & Hernandez-Machado, A. Controlling shapes in a coaxial flow focusing microfluidic device: Experiments and theory. *Micromachines* **11**, (2020).

41. Chiu, Y. J., Cho, S. H., Mei, Z., Lien, V., Wu, T. F. & Lo, Y. H. Universally applicable three-dimensional hydrodynamic microfluidic flow focusing. *Lab Chip* **13**, 1803–1809 (2013).

42. Gale, B. K., Jafek, A. R., Lambert, C. J., Goenner, B. L., Moghimifam, H., Nze, U. C. & Kamarapu, S. K. A review of current methods in microfluidic device fabrication and future commercialization prospects. *Inventions* **3**, (2018).

43. Jolivet, J. P., Chanéac, C. & Tronc, E. Iron oxide chemistry. From molecular clusters to extended solid networks. *Chem. Commun.* **4**, 477–483 (2004).

44. Mascolo, M. C., Pei, Y. & Ring, T. A. Room temperature co-precipitation dynthesis of magnetite nanoparticles in a large ph window with different bases. *Materials (Basel).* **6**, 5549–5567 (2013).

45. Bamshad, A., Nikfarjam, A. & Khaleghi, H. A new simple and fast thermally-solvent assisted method to bond PMMA-PMMA in micro-fluidics devices. *J. Micromechanics Microengineering* **26**, (2016).

46. Rossi, D., Gargiulo, L., Valitov, G., Gavriilidis, A. & Mazzei, L. Experimental characterization of axial dispersion in coiled flow inverters. *Chem. Eng. Res. Des.* **120**, 159–170 (2017).

47. Blonski, S., Domagalski, P. & Kowalewski, T. A. Flow focusing in microfluidic devices. in *19th Polish Fluid Dynamics Conference* (2010).

48. Blanco-Andujar, C., Ortega, D., Pankhurst, Q. A. & Thanh, N. T. K. Elucidating the morphological and structural evolution of iron oxide nanoparticles formed by sodium carbonate in aqueous medium. *J. Mater. Chem.* **22**, 12498–12506 (2012).

49. Suh, Y. K. & Kang, S. A review on mixing in microfluidics. *Micromachines* **1**, 82–111 (2010).

50. Ahn, T., Kim, J. H., Yang, H. M., Lee, J. W. & Kim, J. D. Formation pathways of magnetite nanoparticles by coprecipitation method. *J. Phys. Chem. C* **116**, 6069–6076 (2012).

51. Abou-Hassan, A., Dufrêchfer, J. F., Sandre, O., Mériguet, G., Bernard, O. & Cabuil, V. Fluorescence confocal laser scanning microscopy for Ph mapping in a coaxial flow microreactor: Application in the synthesis of superparamagnetic nanoparticles. *J. Phys. Chem. C* **113**, 18097–18105 (2009).